Unraveling Photoexcited Conformational Changes of Bacteriorhodopsin by Time Resolved Electron Paramagnetic Resonance Spectroscopy

Thomas Rink,* Matthias Pfeiffer,† Dieter Oesterhelt,† Klaus Gerwert,* and Heinz-Jürgen Steinhoff*
*Lehrstuhl für Biophysik, Ruhr-Universität Bochum, 44801 Bochum, and †Max-Planck-Institut für Biochemie, 82152 Martinsried, Germany

ABSTRACT By means of time-resolved electron paramagnetic resonance (EPR) spectroscopy, the photoexcited structural changes of site-directed spin-labeled bacteriorhodopsin are studied. A complete set of cysteine mutants of the C-D loop, positions 100–107, and of the E-F loop, including the first α-helical turns of helices E and F, positions 154–171, was modified with a methanethiosulfonate spin label. The EPR spectral changes occurring during the photocycle are consistent with a small movement of helix C and an outward tilt of helix F. These helix movements are accompanied by a rearrangement of the E-F loop and of the C-terminal turn of helix E. The kinetic analysis of the transient EPR data and the absorbance changes in the visible spectrum reveals that the conformational change occurs during the lifetime of the M intermediate. Prominent rearrangements of nitroxide side chains in the vicinity of D96 may indicate the preparation of the reprotonation of the Schiff base. All structural changes reverse with the recovery of the bacteriorhodopsin initial state.

INTRODUCTION

The retinal protein bacteriorhodopsin (BR) acts as a light-driven proton pump in the cell membrane of *Halobacterium salinarum* (for reviews see, e.g., Lanyi, 1993; Oesterhelt, 1998; Haupts et al., 1999). Cryo-electron microscopy (Henderson et al., 1990; Grigorieff et al., 1996) and x-ray diffraction (Pebay-Peyroula et al., 1997; Lücke et al., 1998, 1999; Essen et al., 1998) revealed its kidney-shaped tertiary structure, consisting of seven transmembrane helices labeled A–G. The chromophore all-*trans* retinal is bound to K216 at helix G via a protonated Schiff base link, constituting a hydrophobic barrier halfway through the proton channel. The absorption of a photon initiates a series of proton transfer reactions inside the protein. These reactions result in a net translocation of one proton into the extracellular space after completion of the catalytic cycle. Intermediates of this cyclic reaction in BR detected by optical spectroscopy are arranged in a photocycle. A widely accepted minimal model consists of a linear sequence of intermediates labeled J, K, L, M, N, and O, most of which have significant back-reactions. The initial step in the photocycle is light-induced isomerization of the retinal to the 13-*cis* configuration. The molecule passes through the short-lived K and L intermediates before the Schiff base becomes deprotonated during the L-to-M transition. This reaction is accompanied by a shift in the absorption maximum to ~410 nm. Fourier transform infrared (FTIR) studies showed that D85 acts as an acceptor for the Schiff base proton (Braiman et al., 1988; Gerwert et al., 1989; Fahmy et al., 1992). In the same instant, a change of the hydrogen bond network causes the appearance of a proton on the extracellular surface of the protein (Rammelsberg et al., 1998), which may possibly be released by a E204/E194 dyad (Essen et al., 1998). A further differentiation of the intermediates occurs in the M state. The M_1 and M_2 states, which have identical absorption maxima in the visible spectrum, can be distinguished by double-flash experiments (Druckmann et al., 1992; Hessling et al., 1997; Nagel et al., 1998). In the transition from M_1 to M_2, the retinal Schiff base is unprotonated and is assumed to change its orientation from the extracellular to the cytoplasmic half of the proton channel (e.g., Schulten and Tavan, 1978; Gerwert and Siebert, 1986; Oesterhelt et al., 1992; Lanyi, 1993). The Schiff base becomes reprotonated in the subsequent M-to-N transition by D96 as a proton donor (Gerwert et al., 1989, Pfefferle et al., 1991; Bousche et al., 1991). Reprotonation of this donor occurs as the photocycle proceeds from N to O, accompanied by the uptake of a proton from the cytoplasm and the reisomerization of the chromophore (Hessling et al., 1993).

A major conformational change in the protein is revealed by diffraction experiments (Dencher et al., 1989; Koch et al., 1991; Nakasako et al., 1991; Subramaniam et al., 1993; Han et al., 1994; Kamikubo et al., 1996; Sass et al., 1997; Oka et al., 1999; Subramaniam et al., 1999; Lücke et al., 1999) as well as infrared spectroscopy (Rothschild et al., 1981; 1993; Gerwert et al., 1990; Souvignier and Gerwert, 1992; Sass et al., 1997). However, its characteristics and mechanism are still obscure. Diffraction experiments yield, in principle, data about the change in the atomic coordinates of the entire protein but suffer from limited time resolution. Hence the authors of these studies had to use mutants to stabilize the intermediate of interest. A common approach is to use D96 replacement mutants (Koch et al., 1991; Subramaniam et al., 1993; Sass et al., 1997; Lücke et al., 1999), as the decay of the M intermediate is prolonged by two orders of magnitude compared to that of the wild type. Likewise, the F171C mutant is used to accumulate the intermediate N (Kamikubo et al., 1996). Other strategies

Received for publication 6 July 1999 and in final form 1 December 1999.
Address reprint requests to Dr. Heinz-Jürgen Steinhoff, Lehrstuhl für Biophysik, Ruhr-Universität Bochum, 44780 Bochum, Germany. Tel.: 49-234-32-24463; Fax: 49-234-32-14626; E-mail: hjs@bph.ruhr-uni-bochum.de.

0006-3495/00/03/1519/12 $2.00

involve arginine solution treatment (Nakasako et al., 1991) and cooling (Han et al., 1994). Despite different approaches, all authors agree on a prominent conformational change in the vicinity of helix G. Furthermore, in the BR mutants as well as in arginine-treated wild type, a tilt of helix F is reported. This movement is visible in the frozen wild type to a smaller extent (Subramaniam et al., 1993). The rise of these conformational changes could not be followed but must occur during the lifetime of the M state because the L intermediate and the initial state do not show significant structural differences (Subramaniam et al., 1999). Time-resolved FTIR studies, on the other hand, give kinetic information on backbone motion based on analysis of the amide bands. The results reveal that the most prominent amide band changes occur during the M-to-N transition (Gerwert et al., 1990; Souvignier and Gerwert, 1992; Hessling et al., 1993; Rothschild et al., 1993). Further detailed analysis of these structural changes is required for a better understanding of the underlying molecular events.

Electron paramagnetic resonance spectroscopy applied to site-directed spin-labeled proteins allows for time-resolved analysis of local conformational changes (Hubbell and Altenbach, 1994; Hubbell et al., 1996). This method has already been used for kinetic studies of the structural dynamics at selected regions of the BR molecule (Steinhoff et al., 1994, 1995; Rink et al., 1997; Mollaaghababa et al., 2000). Conformational changes in the cytoplasmic loops were found to occur during the lifetime of M and during the M-to-N transition. The light-induced change in the spin-spin interaction between two attached nitroxides yielded evidence for a transient opening of the cytoplasmic part of the proton channel (Thorgeirsson et al., 1997).

In the present study, a complete set of spin-labeled cysteine mutants of the C-D loop, positions 100–107, and of the E-F loop, including the first α-helical turns of helices E and F, amino acid positions 154–171, is analyzed by means of time-resolved continuous-wave EPR spectroscopy. We compare the kinetics of the transient EPR signals with the kinetics of the photocycle determined in the visible spectrum to assign the structural changes to the photocycle intermediates. The transient changes in the nitroxide mobility during the photocycle are translated into a model of the structural changes.

MATERIALS AND METHODS

Mutagenesis, expression, and spin labeling were performed as previously described (Pfeiffer et al., 1999; Steinhoff et al., 1999). The spin label (1-oxyl-2,2,5,5-tetramethylpyrroline-3-methyl)methanethiosulfonate (MTSSL) (TRC, Toronto) was covalently attached to the cysteine residues of the membrane-bound BR mutants to yield the spin-labeled side chain R1. Time-resolved continuous-wave EPR experiments were performed using a homemade EPR spectrometer with a homemade TE104 rectangular cavity. This cavity features two sample holes. One of these takes a quartz flat cell (volume 200 μl) containing the BR sample at a concentration of 200–500 μM. A light beam focused into the second hole is reflected onto the sample by a 90° prism mounted inside the cavity. The high transmission of the light path outweighs the drawback of a lower filling factor in our experiments. Spectra were taken at 293 K, with the microwave power set to 1.2 mW. The B-field modulation amplitude was 1.5 G for the continuous-wave spectra and 3 G for time-resolved experiments. Light pulses were generated by a homemade high-energy xenon flash lamp (bulb supplied by ILC Technologies) at ~80 J of electrical energy/pulse and a duration of 30 μs. A 435-nm cutoff filter suppressed undesired secondary photo processes. An infrared filter prevented the sample from transient heating. A remaining artificial EPR signal was compensated for by alternate subtraction of transients recorded inside and outside the paramagnetic resonance. The field switching was done by an additional pair of modulation coils. Depending on the signal-to-noise ratio, between 10^3 and 10^4 transients were averaged for each mutant. The whole setup was controlled by a personal computer, which also performed 12-bit analog-to-digital data acquisition at a sampling rate of up to 20 kHz. The response of the analog electronics to a rectangular input signal was found to be exponential, with a rise time set to either 0.1 or 1 ms.

A sum of exponential functions was fitted to the transient EPR signals, $S(t)$, to characterize the photocycle kinetics. To account for the rise time of the spectrometer, we convoluted the sum of exponentials with the response function of the experimental setup, which yields the function

$$S(t) = \sum_i a_i \frac{\exp(-t/\tau_A) - \exp(-t/\tau_i)}{\tau_A/\tau_i - 1}$$

for $\tau_A \neq \tau_i$. The amplitudes a_i of the relaxation component i and their time constants, τ_i, are the parameters varied during the fit. The time constant τ_A of the response function of the amplifier was fixed to 0.1 ms or 1 ms. Model calculations proved that values of τ_i down to 0.2 ms can be determined, even with an amplifier time constant, τ_A, set to 1 ms.

Absorbance measurements were carried out on a homemade optical bench at 11 wavelengths in the visible (405, 415, 450, 470, 490, 515, 550, 580, 605, 635, and 665 nm). Transient data were sampled between 50 and 2000 times at 12-bit resolution after laser flash excitation at 540 nm. The repetition rate was set between 0.5 s^{-1} and 0.06 s^{-1}, depending on the photocycle duration of the respective mutant. The transients were processed by a global fitting program as described (Rink et al., 1997).

RESULTS

A model of the BR structure based on the data given by Essen et al. (1998) is shown in Fig. 1. Those amino acid positions that were replaced by spin-labeled cysteines are indicated. Residue L100 terminates helix C, and residues V101 to D104 define the cytoplasmic C-D loop. Residues Q105 to T107 form the first α-helical turn of helix D. Positions 154–157 are located at the cytoplasmic end of helix E. Residues 158–165 form the E-F loop. According to these data the residues 166–171 are in helical conformation and form the N-terminus of helix F. The location and orientation of side chains 164–166 were determined from the mobility of the attached nitroxides and their accessibility for paramagnetic quenchers (Pfeiffer et al., 1999). Spin labels attached to engineered cysteine residues in the three cytoplasmic loops were already shown to exhibit spectral changes during the photocycle, which were interpreted as transient conformational changes in the BR molecule (Steinhoff et al., 1994; Rink et al., 1997; Mollaaghababa et al., 2000). Residues with considerable EPR spectral changes

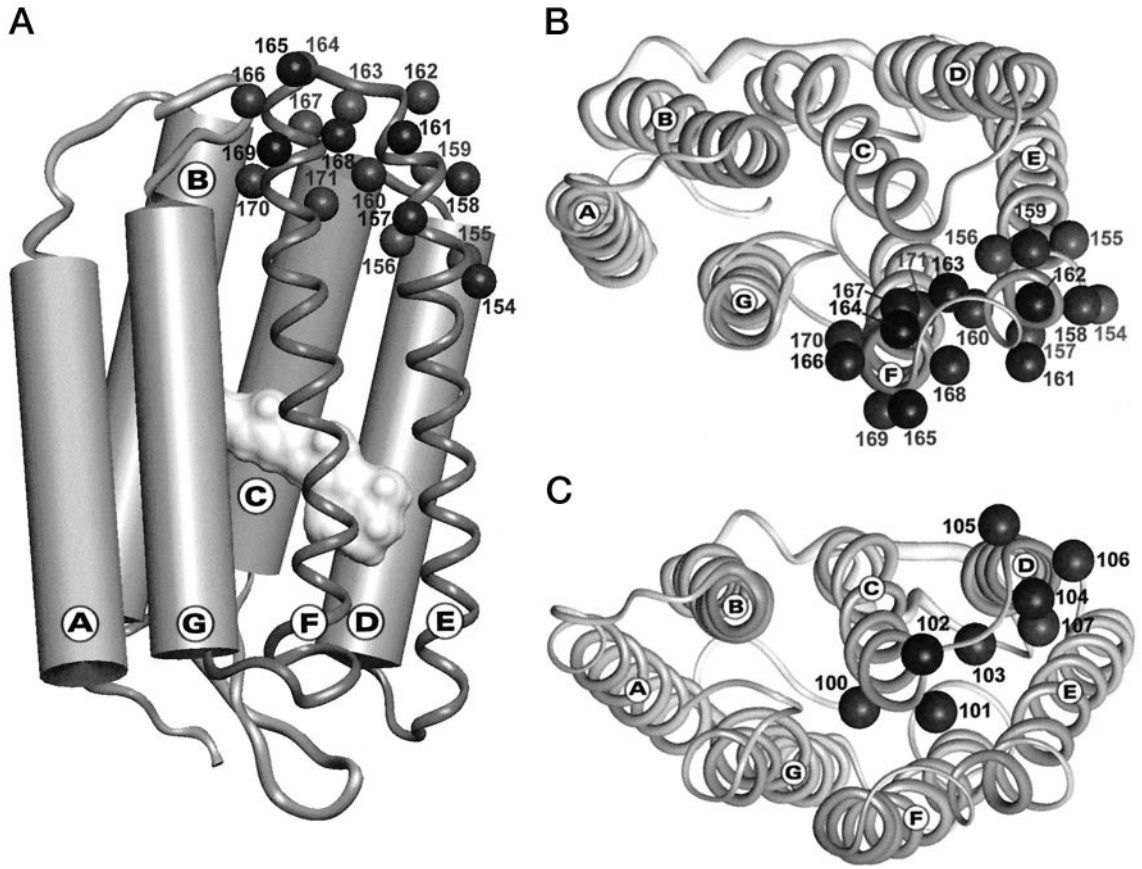

FIGURE 1 Model of the bacteriorhodopsin backbone according to the data of Essen et al. (1998). (*a*) Amino acids that were replaced by cysteines and modified with the spin label MTSSL and the chromophore are indicated. (*b* and *c*) Two views of the cytoplasmic surface show the locations of the modifications in the E-F and C-D loops.

were D36R1 in the A-B loop, V101R1 in the C-D loop, and E161R1 in the E-F loop. No EPR transient could be observed at position 38, most likely because of the lack of N intermediate accumulation in this mutant (Riesle et al., 1996). The absence of any transient EPR signal for the nitroxides attached to position 105 was evidence that helix D is not involved in the structural rearrangement (Steinhoff et al., 1994).

Continuous-wave EPR spectra

The shape of the continuous-wave EPR absorption spectra reflect the molecular motion of the protein-bound nitroxide. The extent of thermal fluctuation of the spin-labeled side chain is limited by its interaction with the local protein environment (Miick et al., 1991, 1993; Todd and Millhauser, 1991; Steinhoff and Hubbell, 1996). Thus static EPR spectra contain information about the tertiary structure and the flexibility of the protein in the immediate vicinity of the bound nitroxide. If the reorientational motion of the spin label is only negligibly restricted by interactions with neighboring atoms of the protein backbone or side chains, the anisotropic components of the *g* and hyperfine tensors are averaged, resulting in a spectrum with narrow linewidth and minimal apparent hyperfine splitting. On the contrary, if the local environment imposes strong restrictions on the nitroxide motion, absorption lines broaden and the apparent hyperfine splitting reaches a maximum.

The continuous-wave EPR spectra of the studied mutants reveal a large variety of motional restriction (cf. Fig. 2, this paper, and figure 2 of Pfeiffer et al., 1999). As expected, strong immobilization of the nitroxide is found for the spin-labeled side chain incorporated into the cytoplasmic ends of the helices C, D, E, and F. The spectra of the nitroxide at position 100 at the C-terminal end of helix C and at positions 106 and 107 in the N-terminal region of helix D show the typical lineshape of a spin label with strong tertiary interaction buried in a highly structured environment (Mchaourab et al., 1996). According to the structure the dynamics of the nitroxide side chain at position 100 is restricted because of interaction with atoms of helix G, while the reorientational motion of the spin label at 107 is

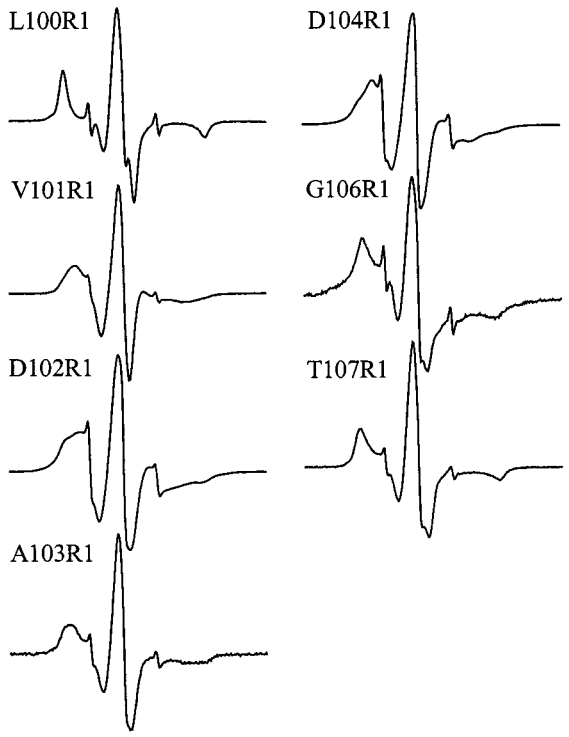

FIGURE 2 Continuous-wave EPR spectra of the MTS spin label attached to the cysteine mutants of the C-D loop region recorded at 293 K. The total scan width is 12.8 mT. A comparison of the linewidth of the center line and the apparent hyperfine splitting reveals a variety of different motional freedom of the nitroxides, depending on the location of the spin label side chain. The EPR spectra for the sequence from F154R1 to F171R1 were presented and discussed in a preceding paper (Pfeiffer et al., 1999).

constrained by helix E (cf. Fig. 1). The nitroxide G106R1 is most likely subject to tertiary interaction with a neighboring BR molecule of the trimer similar to Q105R1 (Steinhoff et al., 1994). The increased mobility of the nitroxide at position 101 reveals the beginning of the loop, in agreement with the structural data. Similar motional freedom is found in the spectra of D102R1, A103R1, and Q105R1. The highest degree of mobility is revealed for the nitroxide located at position 104, where the side chain is oriented toward the aqueous phase. However, the mobility of this side chain is still more restricted than that of side chains D36R1 in the A-B loop (Rink et al., 1997) or S162R1 in the E-F loop (Pfeiffer et al., 1999). This is evidence that the C-D loop is structurally more ordered than the A-B or E-F loops.

EPR spectra that are typical of nitroxides located within well-structured α-helical protein regions are found for spin-labeled residues F154R1, G155R1, T157R1, V167R1, S169R1, T170R1, and F171R1 in the helices E and F, in agreement with the structural data (cf. figure 2 of Pfeiffer et al., 1999). Considerable interaction with the tertiary structure is also revealed for the loop residues A160R1 and M163R1. The nitroxide side chains with the highest mobility are found at the loop positions 159, 161, 162, 164, 165, and 166 (Pfeiffer et al., 1999). Similar spectral shapes are found for spin-labeled BR or lysozyme mutants, in which the cysteines are attached to interhelical loops (Altenbach et al., 1990; Mchaourab et al., 1996; Rink et al., 1997). The high mobility of these side chains is a result of negligible intermolecular and intramolecular contacts and may additionally reflect the high flexibility of the backbone in this loop region. The experimental EPR data are in agreement with the structure of the cytoplasmic ends of helices E and F. The orientation of the side chains of residues 160–164 is supposed to form a turned loop with the side chain of M163R1 oriented toward the proton channel, whereas the nitroxide at position 162 faces the aqueous phase (Pfeiffer et al., 1999).

Absorbance changes in the visible spectrum during the photocycle

The integrity of the structure and function of the spin-labeled cysteine mutants is monitored by means of the analysis of the absorbance change in the visible spectrum. Furthermore, the kinetic characterization of the photocycle provides the basis for the interpretation of the time-resolved EPR experiments in terms of the photocycle intermediates.

The photocycle kinetics were measured at 11 wavelengths in the visible and analyzed by means of a global fitting procedure (Rink et al., 1997). Starting at 1 μs after laser flash excitation, a sum of five exponentials is sufficient to fit the absorbance changes for most of the spin-labeled mutants. The nomenclature of the rates follows that of Hessling et al. (1993). τ_5 and τ_2 describe the biphasic rise of the M intermediate. τ_4 describes the M decay and the rise of N and O, respectively; τ_3 contributes to the decays of M, N, and O, whereas τ_6 is assigned mainly to the decay of the N-intermediate to the BR initial state. For L100R1, V101R1, A103R1, G106R1, T107R1, T170R1, and F171R1 an additional time constant, τ_8, is necessary, which contributes to the recovery of the initial state. The respective values of these time constants are given in Table 1, together with the relative amplitudes of the respective exponentials measured at 415 nm.

As can be seen from the comparison with the wild type, the time constants describing the rise and decay of the intermediate M, τ_2, τ_4, and τ_3, are generally not much altered by the exchange of the native amino acids by spin-labeled cysteines in helix E and in the E-F loop from position 154 to position 166. A significant decrease of the lifetime of the intermediate M (τ_4) to less than 50% of that of the wild type is revealed for L100R1 in helix C and R164R1, V167R1, and T170R1 in helix F. A significant variation of τ_6, which contributes to the recovery of the BR initial state, is found for all mutants. This time constant is

TABLE 1 Time constants of the transients detected in the visible and of the decay of the EPR transients τ_2, τ_3, τ_4, τ_6, and τ_8

Sample	τ_2 (ms)	τ_4 (ms)	τ_3 (ms)	τ_6 (ms)	τ_8 (ms)	τ_c (ms)
Wild type	0.08	2.2 (33%)	7 (67%)	18 (0)	—	—
L100R1	0.08	0.8 (97%)	16 (8%)	100 (−4%)	390 (0)	—
V101R1	0.08	2.6 (34%)	14 (66%)	180 (0)	820 (0)	2.6 ± 0.5 14 ± 2
D102R1	0.09	2.2 (46%)	8 (46%)	71 (8%)	—	—
A103R1	0.10	1.6 (70%)	9 (29%)	86 (2%)	720 (−1%)	0.3 ± 0.2 9.3 ± 1.0
D104R1	0.08	3.5 (50%)	14 (46%)	120 (4%)	—	—
G106R1	0.10	3.2 (12%)	10 (43%)	38 (41%)	240 (4%)	—
T107R1	0.10	2.3 (56%)	12 (26%)	48 (10%)	260 (5%)	—
F154R1	0.08	2.2 (63%)	9 (32%)	63 (5%)	—	0.8 ± 0.3
S158R1	0.08	2.4 (65%)	12 (32%)	100 (3%)	—	0.3 ± 0.2
K159R1	0.09	1.6 (87%)	12 (13%)	120 (0)	—	2.1 ± 0.5
E161R1	0.12	1.8 (56%)	6 (42%)	110 (2%)	—	0.2 ± 0.2
M163R1	0.09	3.3 (61%)	12 (38%)	110 (1%)	—	0.2 ± 0.2
R164R1	0.10	1.1 (85%)	7 (15%)	31 (0)	—	0.7 ± 0.2
E166R1	0.10	1.8 (70%)	12 (27%)	83 (3%)	—	0.9 ± 0.2
V167R1	0.07	1.1 (85%)	4 (15%)	74 (0)	—	0.6 ± 0.3
T170R1	0.06	1.0 (84%)	11 (19%)	110 (2%)	1300 (−5%)	0.3 − 0.2/+0.9
F171R1	0.11	1.4 (75%)	11 (24%)	120 (4%)	820 (−3%)	3 ± 2

The rise of the EPR transient, τ_c, is listed separately. Time constants and amplitudes result from a multiexponential fitting of the absorbance transients measured at 11 different wavelengths. The respective relative amplitudes for a wavelength of 415 nm are given in parentheses. The amplitudes of the exponentials with time constants τ_6 and τ_8 are small for 415 nm but contribute significantly to the recovery of the initial state as measured at 550 nm and 580 nm.

The standard deviations of the time constants determined in the visible spectrum are less than 10%; those of τ_c were determined from the fitting of a complete set of up to 10^4 transients. The time constant representing the fast fraction of the biphasic M rise, τ_5, is found to be between 0.02 and 0.04 ms for wild type and all mutants. The time constants of the photocycle kinetics for the samples with cysteines introduced into the E-F loop that do not show any EPR transient are given by Pfeiffer et al. (1999).

increased up to 10-fold compared to that of the wild type. Significant contributions of τ_8 to the recovery of the initial state are seen for mutations of the C-D loop and of helix F at positions 170 and 171. The amplitudes of the exponentials with time constants τ_6 and τ_8 are small at 415 nm (see Table 1) but determine the absorbance change at 570 nm significantly (not shown).

The contributions of every time constant to the rise and decay of the absorbance at a given wavelength, the amplitude spectra, are similar to that of the wild type for the modifications of helix E and of the E-F loop. A strong negative amplitude of the exponential function characterized by τ_4 is found for V167R1, A168R1, and S169R1 at 550 nm, which is evidence for the accumulation of the N intermediate. In contrast, only a small contribution of τ_4 at 550 nm could be detected for D102R1. A pronounced accumulation of O is visible in the amplitude spectra of D102R1 and T170R1, where the O intermediate is blue shifted. Low O concentrations were found for G155R1, F156R1, and E166R1.

In summary, the influence of the mutation on the photocycle is small in the sequence from 154 to 166. Considerable changes of the photocycle due to the mutations are revealed for T170R1 and F171R1 in helix F, and for the mutants of the C-D loop. These changes involve the intermediates N and O.

EPR spectral changes induced by photoexcitation

Changes in the nitroxide mobility lead to characteristic changes of the first derivative absorption spectra. By means of phase-sensitive detection referenced to a periodic light excitation, the difference spectrum between the BR initial state and excited states can be measured directly (Steinhoff et al., 1994). Within certain spectral ranges, the shape of these difference spectra is unequivocally correlated with a mobility change, as was shown by Rink et al. (1997) by means of spectra simulations with an effective reorientational correlation time as a measure of the nitroxide mobility. Rink et al. (1997) have also shown that the ratios of the transient amplitude changes in the regions of the spectral extremes are a measure of transient mobilization or immobilization of the nitroxide. These effects are distinguishable from changes in the polarity in the vicinity of the spin labels, which mainly alters the hyperfine tensor and leads to considerable spectral changes close to the zero passages of the low and high field lines. For the present study the relative amplitudes of the signal changes were determined for the extremes of the low field and the center lines. A comparison with the results of spectral simulations revealed that the amplitude ratios of observable transients were in agreement with changes in the effective rotational correla-

tion time. Evidence for an additional contribution due to a change in the hyperfine tensor was found for the nitroxide at position 171, which was most probably due to a transient polarity change in the environment of that nitroxide.

Helices C and D and the C-D loop

Transient changes in the spin-labeled side-chain mobility were observed for the nitroxides at positions 101 and 103 in the C-D loop. The B-field-dependent amplitudes of the EPR spectral changes indicate a transient decrease in the nitroxide mobility. This is in agreement with earlier results on these mutants (Steinhoff et al., 1994; Mollaaghababa et al., 2000). Typical EPR transients are shown in Fig. 3. A sum of exponentials was fitted to the EPR data. The amplitudes and time constants of the EPR signal rise were varied, whereas the signal decay was simulated with time constants determined from the kinetic data in the visible spectrum. The effect of the convolution with the response function of the phase-sensitive detector (PSD) was considered as described in Materials and Methods. The integration time of the PSD was set to 1 ms for all samples, with the exception of V167R1, which was measured with an integration time of 0.1 ms. The calculated values of the rise time of the EPR transient, τ_c, are given in Table 1; the contributions of the respective correlation times to the decay of the transient EPR signal are displayed in Fig. 3.

The biphasic rise of the EPR transient of V101R1 occurs with time constants of 2.6 ms and 14 ms. These values are identical to the time constants τ_4 and τ_3 describing the M decay and the rise of the N and O intermediates. The decay of the conformational change is mainly determined by τ_6. The biphasic rise of the structural changes detected at position 103 is fitted with a time constant of 0.3 ms and a small contribution characterized by τ_3. Thus the dominant fraction of the conformational change occurs with a time constant significantly less than the rise of the N intermediate, which was found to be 1.6 ms. The decay of the transient EPR signal is governed by τ_8.

No transient signals could be monitored for the nitroxides at position 100 in helix C, at positions 102 and 104 in the C-D loop, and at positions 106 and 107 in helix D. The absence of any transient spectral changes of L100R1 can be explained by the high motional restriction of the nitroxide side chain already present in the BR initial state. The spectral shape is similar to that of a powder spectrum, and an additional decrease in the mobility would not be visible. The mutation at position 102 seems to inhibit the accumulation of the N intermediate in a manner similar to that of D38R1 (Riesle et al., 1996), as can be judged from the amplitude spectra determined in the visible. Hence, a conformational change that is coupled to the appearance of the N intermediate would not be detectable.

The absence of any detectable conformational changes at positions 104, 106, and 107 is evidence that helix D is not involved in conformational changes. This is in agreement with earlier results, where no transient EPR spectral changes were found for the nitroxide at position 105 (Steinhoff et al., 1994). Thus a movement of helix C or alterations of the interaction of the nitroxide side chain with the E-F loop must be responsible for the increased motional restriction at positions 101 and 103. However, the large distance between the E-F loop and position 103 makes a direct interaction between this side chain and the E-F loop unlikely. Hence a movement of helix C that decreases the flexibility of the C-D loop would account for the EPR data.

Helix E and the E-F loop

Transient EPR spectral changes are observable for the nitroxide at position 154 (Fig. 3). The amplitude of the spectral change indicates a transient increase in the spin-labeled side-chain mobility. The rise of the transient EPR signal occurs with a time constant of 0.8 ms. The M intermediate appears with time constants similar to those of the wild type, 10 μs and 80 μs; the fastest decay of M is given by $\tau_4 = 2.2$ ms. The decay of the EPR signal is determined by τ_3. No transient EPR signals were found for the nitroxides at positions 155, 156, and 157. A transient increase in the nitroxide mobility is found for side chain S158R1. The EPR signal rises with a time constant of 0.3 ms, which is again clearly different from the rise and decay times of the M intermediate. Again, the transient EPR signal disappears with τ_3.

A transient immobilization is detected for the nitroxide at the E-F loop position 159, with a rise time of the EPR transient similar to τ_4. A transient of very small amplitude was found for A160R1 (not shown), which indicated a transient immobilization in agreement with earlier results on that mutant (Mollaaghababa et al., 2000). The rise time of the EPR transient could not be resolved. Transient immobilization with a rise time less than τ_4 was also found for positions 161 and 164. A comparably large transient signal consistent with an increase in the nitroxide mobility is revealed for M163R1 with a rise time of 0.2 ± 0.2 ms. The biphasic decay of the EPR signal of all loop mutants occurs with time constants similar to the values of τ_3 and τ_6. No EPR signal change upon photoexcitation is detected for S162R1, as expected. The high mobility of this side chain in the BR initial state is in agreement with the absence of any tertiary interaction and an orientation of the side chain toward the aqueous phase.

Helix F

The nitroxides at positions 166 and 170 in helix F undergo a transient immobilization upon photoexcitation. The rise time of the transient EPR signal is given by 0.9 ± 0.2 ms for E166R1 and 0.2 ($-0.2/+0.9$) ms for T170R1. The decay of the signal is well fitted by the value of τ_3 for E166R1. In

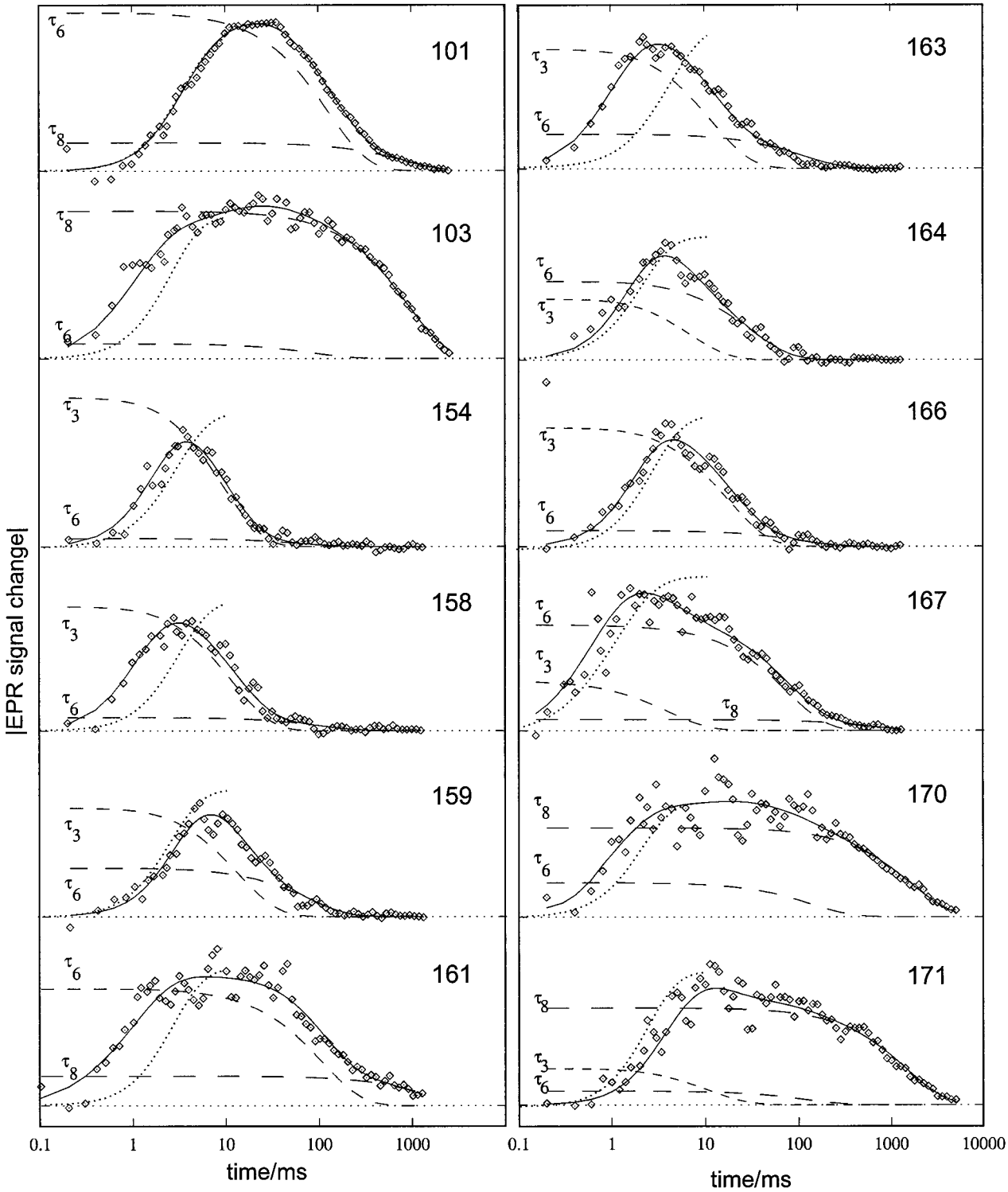

FIGURE 3 EPR signal changes after photoexcitation. The average of 2000 transients of each mutant is shown. Exponential fit curves (*solid lines*) and the dominating time constants, which contribute to the signal decay, are included (*dashed lines*). The dotted lines show the behavior of the fast fraction of the M decay (time constant τ_4), which was determined from measurements of the absorbance changes in the visible spectrum. A convolution with the response function of the EPR spectrometer (PSD time constant set to 0.1 ms for V167R1 and to 1 ms for the other samples) facilitates a direct comparison of the behavior of the M decay with the rise of the EPR transients. The fitted time constants are given in Table 1.

contrast, the recovery of the initial state dynamics of the nitroxide at position 170 is mainly determined by τ_8. The nitroxide side chains of V167R1 and F171R1 in helix F sense a transient decrease in the tertiary interaction. The EPR signals rise with time constants similar to the respective values of τ_4 determined from the study of the photocycle in the visible spectrum. The transient signals decay mainly with the time constants τ_6 (167) and τ_8 (171). No transient EPR spectral changes were detectable for the nitroxides at positions 165, 168, and 169.

DISCUSSION

We have a detailed picture of the proton pathway through the BR molecule, including the specific role of certain amino acids revealed by FTIR spectroscopy. However, the characteristics and the mechanism of the structural change during the photocycle are still subject to discussion. Rearrangement of the α-helices and of the cytoplasmic loops includes a switch after deprotonation on the extracellular side that makes the Schiff base accessible from the cytoplasmic medium. The complete description of these structural changes with high local and time resolution would be the first step toward a structural understanding of such a switch.

The picture of the conformational changes reported in the literature is diverse, most likely because of the different methods used to stabilize the intermediates of interest. Conformational changes in BR were revealed by x-ray and cryoelectron diffraction methods. Using D96 replacement mutants with a prolonged lifetime of the intermediate M, an outward movement of helix F and structural changes within helix G were revealed, which were interpreted as a decreased flexibility of the helix backbone (Dencher et al., 1989; Koch et al., 1991; Subramaniam et al., 1993, 1999; Sass et al., 1997). Small conformational changes were detected in the vicinity of helices B and C. Mutations of F171 provide a BR molecule with a long-lived N intermediate (Kamikubo et al., 1996). The authors observed structural changes close to helices E, F and G. The study of the accumulated O-like intermediate of the mutant L93A revealed structural changes of helices F and G, in agreement with the results mentioned above (Subramaniam et al., 1997). Furthermore, small structural changes close to helices B and C were observed. Diffraction studies of the structure of different intermediates appear to be much more difficult for the wild-type BR because of the limited time resolution of the diffraction experiments. The freeze quenching of a mixture of M and N showed structural changes in the vicinity of helices B and G and evidence for a small tilt of helix F (Subramaniam et al., 1993). Site-directed spin labeling revealed conformational changes of all of the three cytoplasmic interhelical loops during the lifetime of M and during the M-to-N transition (Steinhoff et al., 1994; Rink et al., 1997; Mollaaghababa et al., 2000). Interspin distance measurements within a pair of attached spin labels showed that the E-F loop moves away from both A-B and C-D loops after proton transfer to D85 (Thorgeirsson et al., 1997). Recent x-ray diffraction data of the D96N mutant in the M_N state show that the cytoplasmic ends of helices F and G are disordered between the E-F interhelical loop and residue 176 and beyond residue 222, respectively (Lücke et al., 1999). Compared to the BR initial state, the first residue to move in helix F was found to be V177, displaced 0.16 nm away from the center of the molecule. Notable main-chain movements were resolved within helix G, involving the region from residue 215 to residue 222, most likely a consequence of the strain induced by retinal isomerization.

Changes in the photocycle due to spin labeling

In the analysis of the structural changes the discussion of a possible influence of the spin labeling on the structure and function of BR cannot be excluded. Careful analysis of the photocycle time constants and the amplitude spectra reveals that the functional properties of BR with modifications of helix E and of the E-F loop are only slightly changed compared to the wild type. A considerable change in the reaction rates is revealed for mutations of the C-D loop and helix F. The introduction of a spin-labeled cysteine at positions 101, 103, 170, and 171 leads to a delay of the recovery to the initial state. The decay of the M intermediate is accelerated for R164R1, V167R1, T170R1, and F171R1. This is most probably due to structural influences of the bulky spin label on the initial state structure and the structural relaxation. The side chains of residues V167R1, T170R1, and F171R1 face the interhelical region where the opening occurs (see below). The steric interaction of the nitroxide may tilt helix F out and hence may allow a more rapid reprotonation of the Schiff base. In turn, the uptake of a proton by D96 from the cytoplasmic surface requires an increase in the pK of D96, which may be triggered by the closing of the proton channel. Because this closing may be incomplete for the mutants with the nitroxides attached to the F-helix and to the nearly rigid C-D loop, the reprotonation of D96 is decelerated and the decay of the N intermediate is delayed. This is in agreement with the results of Brown et al. (1995), who used maleimide labels to study the influence of bulky groups after attachment to helix F. In summary, for solvent or lipid-exposed protein surface sites, substitution of the native side chain by R1 produces little change in the photocycle, except for residues that may be of functional importance. This is in agreement with findings of Mchaourab et al. (1996) that solvent-exposed sites and substitution of loop sites by R1 are essentially without effect on enzymatic activity and thermal stability. Even for most of the buried site mutants the effect of R1 on the photocycle is small. Furthermore, the sequence-dependent variation in the EPR lineshapes and in the accessibility of paramagnetic

quenchers to the helical sites is consistent with the expectation based on previously determined BR structures (Grigorieff et al., 1996; Essen et al., 1998; Pfeiffer et al., 1999). Thus the assumption is justified that the information obtained from the transient EPR spectra reflects the changes in the native structure on the level of the side-chain location.

A model of the structural change determined from transient mobility changes of the nitroxides

The transient mobility changes of the nitroxide side chains of the studied mutants are schematically displayed in Fig. 4, where a projection of the cytoplasmic part of BR onto the membrane plane is shown. Two sites on the tertiary interaction surface of helix F, 167 and 171, show a transient increase in mobility, whereas the nitroxides at positions 166 and 170 are transiently immobilized. On the other hand, the nitroxides on the exposed face (165, 168, and 169) show no detectable mobility change. This suggests that the secondary structure of the cytoplasmic end of helix F remains unchanged. According to the structural data and the mobility analysis of the nitroxides (Pfeiffer et al., 1999), the side chains E166R1 and T170R1 are oriented toward helix G, whereas the nitroxides at positions 167 and 171 point toward helices C and E, respectively. A transient increase in the distances between helices F and C and between helices F and E would decrease the tertiary interaction of residues 167 and 171 and thus would account for their transient

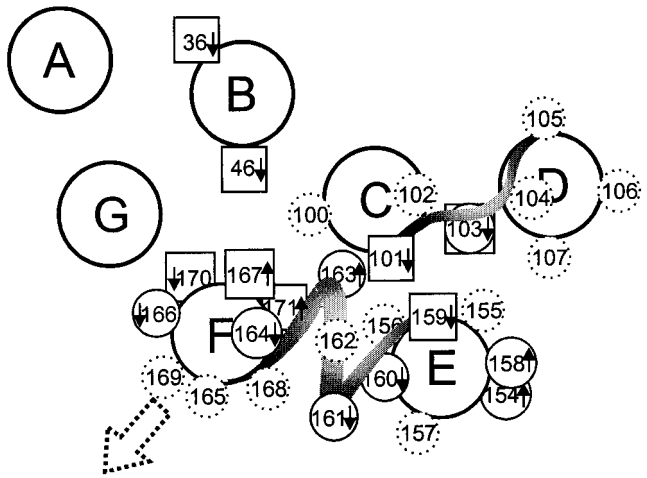

FIGURE 4 Schematic display of the top view of the cytoplasmic structure of BR. The locations of the spin-labeled side chains are shown. The transient increase and decrease in the nitroxide motional freedom during the photocycle are indicated by small arrows pointing upward and downward, respectively. Squares denote spin-labeled side chain positions, where the rise of the conformational change occurs during the M-to-N transition or later, and circles denote positions where the structural change is monitored during the lifetime of the M intermediate. The shapes of the transient spectral changes are in line with an outward movement of helix F and rearrangements of the A-B, C-D, and E-F loops and the C-terminal turn of helix E. Results on D36R1 and T46R1 (Rink et al., 1997) are included.

mobilization. Although the EPR data of V101R1 and A103R1 may indicate a movement of helix C or E, these movements are unlikely to be large, because the nitroxides at position 156 in the contact area between these helices and at position 107 between helices D and E do not show any mobility change. Hence the results point to a transient movement of the cytoplasmic end of helix F away from helix C. The decrease in the mobility of the nitroxides E166R1 and T170R1 indicates a transient strengthening of tertiary interaction between the cytoplasmic parts of helices G and F. This may be a consequence of the movement of helix F away from helix C or of a shift of the cytoplasmic moiety of helix G toward helix F.

A movement of helix F must influence the structure of the E-F loop. The mobility of the spin-labeled side chains attached to the loop positions 159, 161, and 164 is transiently reduced. The underlying conformational change appears to be small, because no spectral change could be detected at position 162 and only small transients were observed for the nitroxide at position 160. The nitroxides at loop positions 159, 161, and 164 are exposed according to their mobility and their accessibility to paramagnetic quenchers (Pfeiffer et al., 1999). According to Mchaourab et al. (1996), backbone dynamics determines the nitroxide mobility for exposed loop positions, although the increased freedom of rotation about the C_α-C_β bond in loops compared to sites in helical structures may also contribute. Thus the observed transient immobilization of the nitroxides at these positions may be the consequence of a transient steric hindrance of rotation about the C_α-C_β bond or, more likely, of a conformational change that reduces the backbone flexibility of the loop. This conformational change is accompanied by an increased mobility of the nitroxide at position 163. This spin-labeled side chain is subject to tertiary interaction and is supposed to be oriented toward the contact interfaces between helices C, E, and F (Pfeiffer et al., 1999). The increased mobility is strong evidence against a movement of helix F toward helix E. In fact, an outward movement of helix F would transiently stretch the E-F loop, increasing the distance between the nitroxide at position 163 and helix C, according to the present structural model. The increased motional freedom at positions 154 and 158 may be the consequence of the F helix movement. The α-helical structure of the C-terminal turn of helix E may be transiently disturbed, leading to a higher flexibility of this part of the helix, which is reflected in an increased dynamics of the spin labels at positions 154 and 158. An outward movement of helix E due to a traction of the E-F loop cannot be excluded. The extent of this movement, however, must be small, because no mobility change was detected at position 157, which was shown to interact with a BR molecule of a neighboring trimer (Pfeiffer et al., 1999). The structural changes detected in helix E at positions 154 and 158 are consistent with the observation of a decreased electron

density in that region (Nakasako et al., 1991; Subramaniam et al., 1993; Kamikubo et al., 1996; Sass et al., 1997).

The present study clearly shows an outward movement of helix F, in agreement with the results of most of the diffraction studies (for a review see, e.g., Haupts et al., 1999). This interpretation of the structural changes is now based on a whole set of spin-labeled mutants. The results found for positions 170 and 171 with a delayed recovery of the BR initial state are strongly supported by the results from mutants V167R1, E166R1, and M163R1, the photocycles of which are only slightly prolonged compared to the wild type. Thus this structural change is not the property of a special mutant, but is most likely a general property of BR. However, the extent of the helix movement might be different for the different mutants.

Movements of helix F and of the terminus of helix E may have an effect on the position of helix C. Evidence for a conformational change close to helix C is given by the transient EPR signal changes of the nitroxides at positions 101 and 103, in agreement with previous studies (Steinhoff et al., 1994; Mollaaghababa et al., 2000). The decrease in nitroxide mobility may be explained by a decrease in the intrinsic flexibility of the C-D loop or the increase in the nitroxide interaction with the nearby tertiary structure. This is again in agreement with diffraction experiments that reveal a decrease in the electron density in the vicinity of the C-D loop and a corresponding increase in the vicinity of helix C, which is evidence for a helix movement during the photocycle (Subramaniam et al., 1993, 1997; Sass et al., 1997).

The time course of the structural change

The results of the diffraction studies of the BR D96N mutant with a delayed M decay show the occurrence of a conformational change during the M intermediate (Subramaniam et al., 1993; Lücke et al., 1999). However, FTIR spectroscopy revealed an intermediate with an unprotonated Schiff base and an N-like protein conformation, which was labeled M_N (Sasaki et al., 1992). In wild-type BR, structures different from the initial state were found under experimental conditions where either the M or the N state should predominate. From this the authors concluded that the observed structural changes are involved in the proposed M_1-to-M_2 transition. X-ray diffraction and FTIR studies of wild-type BR and of the mutant D96N at different degrees of hydration also point to the existence of distinct states in the M intermediate that differ in their conformation (Sass et al., 1997). Double flash experiments were successful in discriminating between two M states differing in the rates for the reprotonation of the Schiff base, which were assigned to the states M_1 and M_2 (Druckmann et al., 1992; Hessling et al., 1997; Nagel et al., 1998). Time-resolved FTIR spectroscopy shows small amide band changes occurring during the M_1-to-M_2 transition, which were interpreted to indicate a movement around the Y185 and P186 peptide bond. However, the most prominent changes in the amide bands and thus the largest peptide backbone movements were found to appear during the M-to-N transition (Souvignier and Gerwert, 1992; Rothschild et al., 1993; Hessling et al., 1993).

The present study shows that the transient EPR signals rise before the M decay for mutants A103R1, S158R1, E161R1, and M163R1 (cf. Fig. 3 and Table 1). Deconvolution of the EPR transients reveals that this is also true for F154R1 and E166R1 (Table 1). For the remaining mutants, V101R1, K159R1, R164R1, T170R1, and F171R1, the decay time of M, τ_4, and the rise time of the conformational change, τ_c, agree within experimental error. Of the transients with rise times faster than τ_4, four can be interpreted as rising with τ_2, the slow rise time of the M intermediate, and may thus be attributed to the L-to-M transition. However, the variance in the fitted values of τ_c does not allow us to exclude the possibility that the conformational change detected in these mutants occurs during the lifetime of the M intermediate. In this case and for the other transients with rise times between τ_2 and τ_4, the explanation of the observed kinetics requires a minimum model with at least two M intermediates of different structures, which we label M_1 and M_2. To explain the variation in the rise time of the structural change, τ_c, for the different mutants we assume that the equilibrium for the M_1-to-M_2-to-N reaction is modulated by the mutation. In mutants where the rate of the M_1 decay exceeds that of the M_2-to-N transition, M_2 is accumulated and the structural change occurs with a time constant of the M_1-to-M_2 transition, the value of which is between the optically determined rise times of M and N, τ_2 and τ_4. If, on the other hand, the rate of the M_2-to-N transition exceeds that of the M_1 decay, M_2 does not accumulate. Hence, the rise time of the structural change should be similar to the rise time of the N intermediate, τ_4. This is found for V101R1, K159R1, V167R1, T170R1, and F171R1. The kinetic data in the visible spectrum do not yield any evidence for a systematic increase in the Schiff base reprotonation rate, strengthening the conclusion that the M_1-to-M_2 transition is delayed for these mutants. It is interesting to note that EPR experiments on the double mutant D96N/V101R1 reveal that the conformational change arises during the M intermediate with a time constant similar to that found for V101R1, whereas the reprotonation of the Schiff base and thus the M-to-N transition are dramatically delayed because of the lack of a proton donor (Mollaaghababa et al., 2000). Our model is in agreement with this observation. However, it cannot be excluded that a sequential occurrence of conformational changes in different parts of the protein contribute to the striking variation in the EPR kinetics with side-chain location (cf. Fig. 4). The movement of helix F, which is accompanied by the rearrangement of the cytoplasmic moieties of helices C, E, and G, occurs before the M decay. This movement is

detected by the nitroxides attached to positions 103, 154, 158, 161, 163, 164, and 166. The corresponding conformational change may be associated with the switch that changes the accessibility of the Schiff base from the extracellular to the cytoplasmic moieties of the proton channel, M_{EC} and M_{CP} (Haupts et al., 1999). Subsequently, a rearrangement of side-chain orientations in the vicinity of D96 takes place. Side-chain locations 46, 101, 159, 167, 170, and 171 are involved in this conformational change, which dominates the observed EPR transients of the respective nitroxides and may report a further tilt of helix F. The presented scheme is in agreement with results of FTIR spectroscopy and diffraction data. Small amide band changes can be seen to develop during the M intermediate. These changes may be associated with alterations of the tertiary structure, as revealed by x-ray and electron diffraction data, which involve changes close to helices B, C, F, and G. The pair of peaks near helix F was suggested to indicate a net outward movement of this helix. The most prominent amide band changes occur during the M-to-N transition (Gerwert et al., 1990; Souvignier and Gerwert, 1992; Rothschild et al., 1993; Sass et al., 1997). These amide band changes may be associated with the structural changes detected by the nitroxides in the vicinity of D96. The underlying structural rearrangement may prepare the transfer of the proton from D96 to the Schiff base and relaxes in a multiphase manner during the remainder of the catalytic cycle.

In conclusion, a detailed picture of the structural changes in the cytoplasmic loops and in the cytoplasmic ends of helices E and F of BR could be developed. Furthermore, this work has enhanced the time resolution of EPR studies of site-directed spin-labeled proteins to the submillisecond time range and thus may expand the range of future applications of this method.

We gratefully acknowledge the support of the Deutsche Forschungsgemeinschaft (SFB 394, C1, C2, and C8 to TR, KG, and H-JS, and SFB 533, A4 to MP and DO).

REFERENCES

Altenbach, C., T. Marti, H. G. Khorana, and W. L. Hubbell. 1990. Transmembrane protein structure: spin labeling of bacteriorhodopsin mutants. *Science.* 248:1088–1092.

Bousche, O., M. Braiman, Y.-W. He, T. Marti, H. G. Khorana, and K. J. Rothschild. 1991. Vibrational spectroscopy of bacteriorhodopsin mutants. *J. Biol. Chem.* 266:11063–11067.

Braiman, M. S., T. Mogi, T. Marti, L. J. Stern, H. G. Khorana, and K. J. Rothschild. 1988. Vibrational spectroscopy of bacteriorhodopsin mutants: light-driven proton transport involves protonation changes of aspartic acid residues. *Biochemistry.* 27:8516–8520.

Brown, L. S., G. Varo, R. Needleman, and J. K. Lanyi. 1995. Functional significance of a protein conformation change at the cytoplasmic end of helix F during the bacteriorhodopsin photocycle. *Biophys. J.* 69: 2103–2111.

Dencher, N., G. Dresselhaus, G. Zaccai, and G. Büldt. 1989. Structural changes in bacteriorhodopsin during photon translocation revealed by neutron diffraction. *Proc. Natl. Acad. Sci. USA.* 86:7876–7879.

Druckmann, S., N. Friedmann, J. K. Lanyi, R. Needleman, M. Ottolenghi, and M. Shewes. 1992. The back photoreaction of the M intermediate in the photocycle of bacteriorhodopsin: mechanism and evidence for two M species. *Photochem. Photobiol.* 56:1041–1047.

Essen, L. O., R. Siegert, W. D. Lehmann, and D. Oesterhelt. 1998. Lipid patches in membrane protein oligomeres: crystal structure of the bacteriorhodopsin-lipid complex. *Proc. Natl. Acad. Sci. USA.* 95: 11673–11678.

Fahmy, K., O. Weidlich, M. Engelhardt, J. Tittor, D. Oesterhelt, and F. Siebert. 1992. Indentification of the proton acceptor of Schiff base deprotonation in bacteriorhodopsin: a Fourier-transform infrared study on the mutant $Asp^{85}\rightarrow Glu$ in its natural lipid environment. *Photochem. Photobiol.* 56:1073–1083.

Gerwert, K., B. Hess, J. Soppa, and D. Oesterhelt. 1989. The role of Asp^{96} in the proton pump mechanism of bacteriorhodopsin. *Proc. Natl. Acad. Sci. USA.* 86:4943–4947.

Gerwert, K., and F. Siebert. 1986. Evidence for light induced 13-*cis*, 14-s-*cis* isomerization in bacteriorhodopsin obtained by FTIR difference spectroscopy using isotopically labelled retinals. *EMBO J.* 5:805–811.

Gerwert, K., G. Souvignier, and B. Hess. 1990. Simultaneous monitoring of light-induced changes in protein side group protonation, chromophore isomerization and backbone motion of bacteriorhodopsin by time-resolved Fourier-transform infrared spectroscopy. *Proc. Natl. Acad. Sci. USA.* 87:9774–9778.

Grigorieff, N., T. A. Ceska, K. H. Downing, J. M. Baldwin, and R. Henderson. 1996. Electron-crystallographic refinement of the structure of bacteriorhodopsin. *J. Mol. Biol.* 259:393–421.

Han, B.-G., J. Vonck, and R. M. Glaeser. 1994. The bacteriorhodopsin photocycle: direct structural study of two substates of the M-intermediate. *Biophys. J.* 67:1179–1186.

Haupts, U., J. Tittor, and D. Oesterhelt. 1999. Closing in on bacteriorhodopsin: progress in understanding the molecule. *Annu. Rev. Biophys. Biomol. Struct.* 28:367–399.

Henderson, R., J. M. Baldwin, T. A. Ceska, F. Zemlin, E. Beckmann, and K. H. Downing. 1990. Model for the structure of bacteriorhodopsin based on high-resolution electron cryo-microscopy. *J. Mol. Biol.* 213: 899–929.

Hessling, B., J. Herbst, R. Rammelsberg, and K. Gerwert. 1997. Fourier transform infrared double-flash experiments resolve bacteriorhodopsin's M1 to M2 transition. *Biophys. J.* 73:2071–2080.

Hessling, B., G. Souvignier, and K. Gerwert. 1993. A model-independent approach to assigning bacteriorhodopsin's intramolecular reactions to photocycle intermediates. *Biophys. J.* 65:1929–1941.

Hubbell, W. L., and C. Altenbach. 1994. Investigation of structure and dynamics in membrane proteins using site-directed spin labeling. *Curr. Opin. Struct. Biol.* 4:566–573.

Hubbell, W. L., H. S. Mchaourab, C. Altenbach, and M. A. Lietzow. 1996. Watching proteins move using site-directed spin labeling. *Structure.* 4:779–783.

Kamikubo, H., M. Kataoka, G. Varo, T. Oka, F. Tokunaga, R. Needleman, and J. Lanyi. 1996. Structure of the N-intermediate of bacteriorhodopsin revealed by x-ray diffraction. *Proc. Natl. Acad. Sci. USA.* 93: 1386–1390.

Koch, M. H. J., N. A. Dencher, D. Oesterhelt, H. J. Plöhn, G. Rapp, and G. Büldt. 1991. Time-resolved x-ray diffraction study of structural changes associated with the photocycle of bacteriorhodopsin. *EMBO J.* 10: 521–526.

Lanyi, J. 1993. Proton translocation mechanism and energetics in the light driven pump bacteriorhodopsin. *Biochim. Biophys. Acta.* 1183:241–261.

Lücke, H., H.-T. Richter, and J. K. Lanyi. 1998. Proton transfer pathways in bacteriorhodopsin at 2.3 angstrom resolution. *Science.* 280: 1934–1937.

Lücke, H., B. Schobert, H.-T. Richter, J.-P. Cartailler, J. K. Lanyi. 1999. Structural changes in bacteriorhodopsin during ion transport at 2 Angstrom resolution. *Science.* 286:255–260.

Mchaourab, H. S., M. A. Lietzow, K. Hideg, and W. L. Hubbell. 1996. Motion of spin-labeled side chains in T4 lysozyme. Correlation with protein structure and dynamics. *Biochemistry.* 35:7692–7704.

Miick, S. M., K. M. Casteel, and G. L. Millhauser. 1993. Experimental molecular dynamics of an alanine-based helical peptide determined by spin label electron spin resonance. *Biochemistry.* 32:8014–8021.

Miick, S. M., A. P. Todd, and G. L. Millhauser. 1991. Position-dependent local motions in spin-labeled analogues of a short α-helical peptide determined by electron spin resonance. *Biochemistry.* 30:9498–9503.

Mollaaghababa, R., H.-J. Steinhoff, W. L. Hubbell, and H. G. Khorana. 2000. Time-resolved site-directed spin-labeling studies of bacteriorhodopsin: loop-specific conformational changes in M. *Biochemistry*. In press.

Nagel, G., B. Kelety, B. Möckel, G. Büldt, and E. Bamberg. 1998. Voltage dependence of proton pumping by bacteriorhodopsin is regulated by the voltage-sensitive ratio of M_1 to M_2. *Biophys. J.* 74:403–412.

Nakasako, M., M. Kataoka, Y. Amemiya, and F. Tokunaga. 1991. Crystallographic characterization by x-ray diffraction of the M-intermediate from the photo-cycle of bacteriorhodopsin at room temperature. *FEBS Lett.* 292:73–75.

Oesterhelt, D. 1998. Structure and mechanism of the family of retinal proteins from halophilic archaea. *Curr. Opin. Struct. Biol.* 8:489–500.

Oesterhelt, D., J. Tittor, and E. Bamberg. 1992. A unifying concept for ion translocation by retinal proteins. *J. Bioenerg. Biomembr.* 24:181–191.

Oka, T., H. Kamikubo, F. Tokunaga, J. Lanyi, R. Needleman, and M. Kataoka. 1999. Conformation change of helix G in the bacteriorhodopsin photocycle: investigation with heavy atom labeling and x-ray diffraction. *Biophys. J.* 76:1018–1023.

Pebay-Peyroula, E., G. Rummel, J. P. Rosenbusch, and E. M. Landau. 1997. X-ray structure of bacteriorhodopsin at 2.5 Angstroms from microcrystals grown in lipid cubic phases. *Science.* 277:1676–1681.

Pfefferle, J. M., A. Maeda, J. Sasaki, and T. Yozikawa. 1991. Fourier transform infrared study of the N intermediate of bacteriorhodopsin. *Biochemistry.* 30:6548–6556.

Pfeiffer, M., T. Rink, K. Gerwert, D. Oesterhelt, and H.-J. Steinhoff. 1999. Site-directed spin labeling reveals the orientation of the amino acid side chains in the E-F loop of bacteriorhodopsin. *J. Mol. Biol.* 287:163–171.

Rammelsberg, R., G. Huhn, M. Lübben, and K. Gerwert. 1998. Bacteriorhodopsin's intramolecular proton-release pathway consists of a hydrogen-bonded network. *Biochemistry.* 37:5001–5009.

Riesle, J., D. Oesterhelt, N. A. Dencher, and J. Heberle. 1996. D38 is an essential part of the proton translocation pathway in bacteriorhodopsin. *Biochemistry.* 35:6635–6643.

Rink, T., J. Riesle, D. Oesterhelt, K. Gerwert, and H.-J. Steinhoff. 1997. Spin-labeling studies of the conformational changes in the vicinity of D36, D38, T46 and E161 of bacteriorhodopsin during the photocycle. *Biophys. J.* 73:983–993.

Rothschild, K. J., T. Marti, S. Sonar, Y.-W. He, P. Rath, W. Fischer, and H. G. Khorana. 1993. Asp^{96} deprotonation and transmembrane α-helical structural changes in bacteriorhodopsin. *J. Biol. Chem.* 268: 27046–27052.

Rothschild, K. J., M. Zagaeski, and W. A. Cantore. 1981. Conformational changes of bacteriorhodopsin detected by Fourier transform infrared difference spectroscopy. *Biochem. Biophys. Res. Commun.* 103: 483–489.

Sasaki, J., Y. Shichida, J. K. Lanyi, and A. Maeda. 1992. Protein changes associated with reprotonation of the Schiff base in the photocycle of $Asp^{96} \rightarrow$Asn bacteriorhodopsin. The M_N intermediate with unprotonated Schiff base but N-like protein structure. *J. Biol. Chem.* 267: 20782–20786.

Sass, H.-J., I. W. Schachowa, G. Rapp, M. H. J. Koch, D. Oesterhelt, G. Büldt, and N. Dencher. 1997. The tertiary structural changes in bacteriorhodopsin occur during M states: x-ray diffraction and and Fourier transform infrared spectroscopy. *EMBO J.* 16:1484–1491.

Schulten, K., and P. Tavan. 1978. A mechanism for the light-driven proton pump of *Halobacterium halobium. Nature.* 272:85–86.

Souvignier, G., and K. Gerwert. 1992. Proton uptake mechanism of bacteriorhodopsin as determined by time-resolved spectroscopic FTIR spectroscopy. *Biophys. J.* 63:1393–1405.

Steinhoff, H.-J., and W. L. Hubbell. 1996. Calculation of electron paramagnetic resonance spectra from Brownian dynamics trajectories: application to nitroxide side chains in proteins. *Biophys. J.* 71:2201–2212.

Steinhoff, H.-J., R. Mollaaghababa, C. Altenbach, K. Hideg, M. Krebs, H. G. Khorana, and W. L. Hubbell. 1994. Time-resolved detection of structural changes during the photocycle of spin-labeled bacteriorhodopsin. *Science.* 266:105–107.

Steinhoff, H.-J., R. Mollaaghababa, C. Altenbach, H. G. Khorana, and W. L. Hubbell. 1995. Site directed spin labeling studies of structure and dynamics in bacteriorhodopsin. *Biophys. Chem.* 56:89–94.

Steinhoff, H.-J., M. Pfeiffer, T. Rink, O. Burlon, M. Kurz, J. Riesle, E. Heuberger, K. Gerwert, and D. Oesterhelt. 1999. Azide reduces the hydrophobic barrier of the bacteriorhodopsin proton channel. *Biophys. J.* 76:2702–2710.

Subramaniam, S., A. R. Faruqi, D. Oesterhelt, and R. Henderson. 1997. Electron diffraction studies of light-induced conformational changes in the Leu-93-Ala bacteriorhodopsin mutant. *Proc. Natl. Acad. Sci. USA.* 94:1767–1772.

Subramaniam, S., M. Gerstein, D. Oesterhelt, and R. Henderson. 1993. Electron diffraction analysis of structural changes in the photocycle of bacteriorhodopsin. *EMBO J.* 12:1–8.

Subramaniam, S., I. Lindahl, P. Bullough, A. R. Faruqi, J. Tittor, D. Oesterhelt, L. Brown, J. Lanyi, and R. Henderson. 1999. Protein conformational changes in the bacteriorhodopsin photocycle. *J. Mol. Biol.* 287:145–161.

Thorgeirsson, T. E., W. Xiao, L. S. Brown, R. Needleman, J. K. Lanyi, and Y.-K. Shin. 1997. Transient channel-opening in bacteriorhodopsin: an EPR study. *J. Mol. Biol.* 273:951–957.

Todd, A. P., and G. L. Millhauser. 1991. ESR spectra reflect local and global mobility in a short spin-labeled peptide throughout the α-helix-coil transition. *Biochemistry.* 30:5515–5523.